The deubiquitinase Ubp3/Usp10 constrains glucose-mediated mitochondrial repression via phosphate budgeting

Vineeth Vengayil[1,2], Shreyas Niphadkar[1,2], Swagata Adhikary[1,2], Sriram Varahan[1], Sunil Laxman[1]*

1. Institute for Stem Cell Science and Regenerative Medicine (DBT-inStem)
   GKVK Post Bellary Road
   Bangalore 560065
2. Manipal Academy of Higher Education, Manipal, Karnataka 576104, India

*correspondence: sunil@instem.res.in

Keywords: mitochondria, glycolysis, phosphate, deubiquitinase, Crabtree

Abstract

Many cells in high glucose repress mitochondrial respiration, as observed in the Crabtree and Warburg effects. Our understanding of biochemical constraints for mitochondrial activation is limited. Using a *Saccharomyces cerevisiae* screen, we identified the conserved deubiquitinase Ubp3 (Usp10), as necessary for mitochondrial repression. Ubp3 mutants have increased mitochondrial activity despite abundant glucose, along with decreased glycolytic enzymes, and a rewired glucose metabolic network with increased trehalose production. Utilizing *Δubp3* cells, along with orthogonal approaches, we establish that the high glycolytic flux in glucose continuously consumes free Pi. This restricts mitochondrial access to inorganic phosphate (Pi), and prevents mitochondrial activation. Contrastingly, rewired glucose metabolism with enhanced trehalose production and reduced GAPDH (as in *Δubp3* cells) restores Pi. This collectively results in increased mitochondrial Pi and derepression, while restricting mitochondrial Pi transport prevents activation. We therefore suggest that glycolytic-flux dependent intracellular Pi budgeting is a key constraint for mitochondrial repression.

Introduction

Rapidly proliferating cells have substantial metabolic and energy demands in order to increase biomass (1, 2). This includes a high ATP demand, obtained from cytosolic glycolysis or mitochondrial oxidative phosphorylation (OXPHOS), to fuel multiple reactions (3). Interestingly, many rapidly proliferating cells preferentially rely on ATP from glycolysis/fermentation over mitochondrial respiration even in oxygen-replete conditions, and is the well-known Warburg effect (4, 5). Many such cells repress mitochondrial processes in high glucose, termed glucose-mediated mitochondrial repression or the Crabtree effect (6, 7). This is observed in some tumors (5), neutrophils (8), activated macrophages (9), stem cells (10–12), and famously *Saccharomyces cerevisiae* (7). Numerous studies have identified signaling programs or regulators of glucose-mediated mitochondrial repression. However, biochemical programs and regulatory processes in biology evolve around key biochemical constraints (13). The biochemical constraints for mitochondrial repression remain unresolved (14, 15).

There are two hypotheses on the biochemical principles driving mitochondrial repression. The first proposes direct roles for glycolytic intermediates in driving mitochondrial respiration, by inhibiting specific mitochondrial outputs (16, 17). The second hypothesizes that a competition between glycolytic and mitochondrial processes for mutually required metabolites/co-factors such as pyruvate, ADP or inorganic phosphate (Pi) could determine the extent of mitochondrial repression (14, 15, 18). These are not all mutually exclusive, and a combination of these factors might dictate mitochondrial repression in high glucose. However, any hierarchies of importance are unclear (19), and experimental data for the necessary constraints for mitochondrial repression remains incomplete.

One approach to resolve this question has been to identify regulators of metabolic state under high glucose. Post-translational modifications (PTMs) regulated by signaling systems can regulate mitochondrial repression (20–22). Ubiquitination is a PTM that regulates global proteostasis (23, 24), but the roles of ubiquitination-dependent processes in regulating mitochondrial repression are poorly explored. Ubiquitination itself is determined by the balance between ubiquitination, and deubiquitinase (DUB) dependent deubiquitination (25). Little is known about the roles of DUBs in regulating metabolic states, making the DUBs interesting candidate regulators of mitochondrial repression.

63 In this study, using an *S. cerevisiae* DUB knock-out library-based screen, we identified
64 the evolutionarily conserved deubiquitinase Ubp3 (mammalian Usp10) as required for
65 mitochondrial repression in high glucose. Loss of Ubp3 resulted in mitochondrial activation,
66 along with a reduction in the glycolytic enzymes-phosphofructokinase 1 (Pfk1) and GAPDH
67 (Tdh2 and Tdh3). This consequently reroutes glucose flux and increases trehalose
68 biosynthesis. This metabolic rewiring increases Pi release from trehalose synthesis, and
69 decreases Pi consumption in glycolysis, to cumulatively increase Pi pools. Using *ubp3Δ* cells
70 along with independent analysis of wild-type cells, and isolated mitochondrial fractions, we
71 establish that glycolytic-flux dependent Pi allocations to mitochondria determines
72 mitochondrial activity. Through these data, we propose how intracellular Pi balance as
73 controlled by glycolytic flux, is a biochemical constraint for mitochondrial repression.

74 **Results**

75 **A deubiquitinase deletion screen identifies Ubp3 as a regulator of glucose-mediated**
76 **mitochondrial repression**

77 In cells such as *S. cerevisiae*, high glucose represses mitochondrial activity as well as
78 OXPHOS-dependent ATP synthesis (7, 26) (illustrated in Figure 1A). Our initial objective was
79 to identify proteostasis regulators of glucose-mediated mitochondrial repression. We
80 generated and used a deubiquitinase (DUB) deletion strain library of *S. cerevisiae* (Figure S1A),
81 to unbiasedly identify regulators of mitochondrial repression by measuring the fluorescence
82 intensity of a potentiometric dye Mitotracker CMXRos (illustrated in Figure 1B). Using this
83 screen, we identified DUB mutants with altered mitochondrial membrane potential (Figure
84 1C, Figure S1A). Note: WT cells in a respiratory medium (2% ethanol) were used as a control
85 to estimate maximum mitotracker fluorescence intensity (Figure S1B).

86 A prominent 'hit' was the evolutionarily conserved deubiquitinase Ubp3 (Figure 1C),
87 (homologous to mammalian Usp10) (Figure S1C). Due to its high degree of conservation
88 across eukaryotes (Figure S1C) as well as putative roles in metabolism or mitochondrial
89 function (27–29), we focused our further attention on this DUB. Cells lacking Ubp3 showed
90 an ~1.5-fold increase in mitotracker fluorescence (Figure 1C, Figure S1A). Cells with
91 catalyticaly inactive Ubp3 ($Ubp3^{C469A}$), showed increased mitochondrial potential comparable

92 to *ubp3Δ* (Figure 1D). This data confirmed that Ubp3 catalytic activity of is required to fully
93 repress mitochondrial activity under high glucose. The catalytic site mutation did not affect
94 steady-state Ubp3 levels (Figure S1D).

95 Next, to assess the requirement of Ubp3 for mitochondrial function, we quantified the
96 electron transport chain (ETC) complex IV subunit Cox2 (30)(Figure 1E). *ubp3Δ* had higher
97 Cox2 than WT (Figure 1E). There was no increase in mitochondrial outer membrane protein
98 Tom70 (Figure S1E), suggesting that the increased Cox2 is not merely because of higher total
99 mitochondrial content. We next measured the basal oxygen consumption rate (OCR) of
100 *ubp3Δ*, and basal OCR was higher in *ubp3Δ*, indicating higher respiration (Figure 1F).

101 Next, we asked if mitochondrial ATP synthesis was higher in *ubp3Δ*. The total ATP
102 levels in WT and *ubp3Δ* were comparable (Figure 1G). However, upon treatment with the ETC
103 complex IV inhibitor sodium azide, ATP levels in WT were higher than *ubp3Δ*, contributing to
104 ~60% of the total ATP (Figure 1H). In contrast, the ATP levels in *ubp3Δ* after sodium azide
105 treatment were ~ 40% of the total ATP (Figure 1H). These data suggest a higher contribution
106 of mitochondrial ATP synthesis towards the total ATP pool in *ubp3Δ*.

107 We next asked if *ubp3Δ* required higher mitochondrial activity for growth. In high
108 glucose, WT show minimal growth inhibition in the presence of sodium azide, indicating lower
109 reliance on mitochondrial function (Figure 1I). Contrastingly, *ubp3Δ* or Ubp3^{C469A} show a
110 severe growth defect in the presence of sodium azide (Figure 1I). Deletion of ETC components
111 Cox2, and the ATP synthase subunits Atp1 and Atp10 results in a severe growth defect in
112 *ubp3Δ* compared to WT (Figure S1F). Together, these results indicate that the loss of Ubp3
113 makes cells dependent on mitochondrial ATP synthesis in high glucose.

114 Collectively these data show that in 2% glucose, *ubp3Δ* have high mitochondrial
115 activity, respiration, and rely on this mitochondrial function for ATP production and growth.
116 We therefore decided to use *ubp3Δ* cells to start delineating requirements for glucose-
117 mediated mitochondrial repression.

118

119 **Key glycolytic enzymes decrease and glucose flux is rerouted in *ubp3Δ* cells**

120 Glucose-6 phosphate (G6P) is the central node in glucose metabolism where carbon-
121 allocations are made towards distinct metabolic arms, primarily: glycolysis, the pentose
122 phosphate pathway (PPP), and trehalose biosynthesis (Figure 2A). We first compared
123 amounts of two key ('rate-controling') glycolytic enzymes - Phosphofructokinase 1 (Pfk1),
124 GAPDH isozymes (Tdh2, Tdh3) (3), along with the enolase isozymes (Eno1, Eno2) in WT and
125 *ubp3Δ* cells. Pfk1, Tdh2, and Tdh3 substantially decreased in *ubp3Δ* (but not Eno1 and Eno2)
126 (Figure 2B, S2A). Since deubiquitinases can control protein amounts by regulating
127 proteasomal degradation, we asked if the decrease in Pfk1, Tdh2 and Tdh3 in *ubp3Δ* is due to
128 proteasomal degradation. To test this, we measured the levels of these enzymes in *ubp3Δ*
129 after treatement with proteasomal inhibitor MG132. We did not observe any rescue in the
130 levels of these enzymes in MG132 treated samples, suggesting that the decreased levels of
131 these enzymes were not due to increased proteasomal degradation (Figure S2B). To further
132 understand if these enzyme transcripts are altered in *ubp3Δ*, we measured the mRNA levels
133 of PFK1, TDH2 and TDH3 in WT, *ubp3Δ* and Ubp3^{C469A} cells. The transcripts of all the three
134 genes in *ubp3Δ* and Ubp3^{C469A} cells decreased (Figure S2C), suggesting that Ubp3 regulates
135 the transcripts of these glycolytic enzyme genes. The reduction in the Pfk and GAPDH enzyme
136 amounts was intriguing, because the Pfk and GAPDH steps are critical in determining
137 glycolytic flux (3, 31). A reduction in these enzymes could therefore decrease glycolytic flux,
138 and would reroute glucose (G6P) allocations via mass action towards other branches of
139 glucose metabolism, primarily the pentose phosphate pathway as well as trehalose
140 biosynthesis (Figure 2A). To assess this, we first measured the steady-state levels of key
141 glycolytic and pentose phosphate pathway (PPP) intermediates, and trehalose in WT or *ubp3Δ*
142 using targeted LC-MS/MS. Glucose-6/fructose-6 phosphate (G6P/F6P) increased in *ubp3Δ*
143 (Figure 2C). Concurrently, trehalose, and the PPP intermediates ribose 5-phosphate (R5P) and
144 sedoheptulose 7-phosphate (S7P), increased in *ubp3Δ* (Figure 2C).

145 Since steady-state metabolite amounts cannot separate production from utilization,
146 in order to unambiguously assess if glycolytic flux is reduced in *ubp3Δ* cells, we utilized a pulse
147 labeling of $^{13}C_6$ glucose, following which the label incorporation into glycolytic and other
148 intermediates was measured. Note that because glycolytic flux is very high in yeast, this
149 experiment would require rapid pulsing and extraction of metabolites in order to stay in a
150 linear range and avoid label saturation. We therefore established a very short time point of

151 label-addition, quenching and metabolite extraction post ^{13}C glucose pulse. Since flux
152 saturates/reaches steady-state in seconds, we first ensured that the label incorporation into
153 individual metabolites after the ^{13}C glucose pulse was in the linear range, and for early
154 glycolytic intermediates this was seconds after glucose addition. This new methodology is
155 extensively described in materials and methods, with required controls shown in Figure S2E.
156 WT and *ubp3Δ* cells were grown in high glucose, pulsed with $^{13}C_6$ glucose, and the relative ^{13}C
157 label incorporation into glycolytic intermediates and trehalose were measured, as shown in
158 the schematic (Figure S2D). In *ubp3Δ,* ^{13}C label incorporation into G6P/F6P as well as trehalose
159 substantially increased (Figure 2D). Contrastingly, ^{13}C label incorporation into glycolytic
160 intermediates F1,6BP, G3P, 3PG and PEP decreased, indicating decreased glycolytic flux
161 (Figure 2D). We next measured ethanol concentrations and production rates, as an additional
162 output of relative glycolytic rates. We observed decreased steady-state ethanol levels, as well
163 as ethanol production rates in *ubp3Δ* (Figure 2F).

164 Collectively, these results reveal that that reduced Pfk1 and GAPDH (in *ubp3Δ*)
165 decrease glucose flux via glycolysis, which results in rewired glucose flux towards trehalose
166 biosynthesis and the PPP.

167

168 **Rerouted glucose flux results in phosphate (Pi) accumulation**

169 We therefore asked if the proteomic state, as observed in *ubp3Δ* cells, could provide
170 clues to explain the coupling between mitochondrial derepression and rerouted glucose flux.
171 A recent study by Isasa et al., had systematically quantified the changes in protein levels in
172 *ubp3Δ* cells (28). We therefore reanalyzed this extensive dataset, looking for changes in
173 proteins that would correlate with these metabolic processes. Notably, we observed
174 increased levels of proteins of the mitochondrial ETC and respiration, and decreased amounts
175 of glucose metabolizing enzymes in *ubp3Δ* (Figure 3A). Additionally, multiple proteins
176 involved in regulating phosphate (Pi) homeostasis were decreased in *ubp3Δ* (Figure 3A) (28).
177 We had recently uncovered a reciprocal coupling of Pi homeostasis with the different arms of
178 glucose metabolism, particularly trehalose biosynthesis (32, 33), and therefore wondered if a

179 glycolytic-flux dependent change in Pi homeostatsis had any role in mitochondrial respiration.
180 Our hypothesis was refined based on the reasoning given below.

181 One explanation for mitochondrial repression can be an internal competition for
182 shared metabolites/co-factors between (cytosolic) glycolytic and mitochondrial processes,
183 that mitochondria might not be sufficiently able to access (14, 18, 19). In this context, a
184 plausible role for inorganic phosphate (Pi) in regulating mitochondrial repression can be
185 hypothesized. Cytosolic glycolysis requires rapid, high consumption of net Pi (19, 34, 35), and
186 this could possibly limit the Pi that is continuously available for mitochondrial use (18, 36),
187 thereby repressing mitochondria. Contextually, the balance between reactions releasing vs
188 consuming Pi could explain changes in global Pi levels (33). A continuous hub of Pi
189 consumption is glycolysis. Here, GAPDH catalyzes G3P to 1,3BPG, converting ADP to ATP,
190 while concurrently consuming a molecule of Pi (35, 37). This Pi that goes into ATP will
191 subsequently be used for nucleotide biosynthesis, polyphosphate biosynthesis and protein
192 phosphorylation (33, 38). Therefore, we can surmise that in high glycolytic flux, the
193 production of ATP, nucleotides and polyphosphates is concurrent with Pi consumption (37,
194 39, 40). Could this reaction therefore limit cytosolic Pi for the mitochondria (as illustrated in
195 Figure 3B)? Notably, *ubp3Δ* have reduced GAPDH levels and decreased glycolytic flux. Second,
196 trehalose synthesis is a Pi releasing reaction, and a major source of free Pi that is critical for
197 Pi homeostasis (32, 35). Flux through this reaction is also substantially higher in *ubp3Δ*.
198 Therefore, these cells might have increased Pi release (via trehalose), coupled with
199 decreased Pi consumption (via decreased GAPDH). We therefore asked if total Pi increases in
200 *ubp3Δ* (Figure 3B)?

201 To test this, we directly assessed total Pi levels in *ubp3Δ* and WT. *ubp3Δ* cells had
202 higher Pi than WT, and this was comparable to Pi in WT grown in excess Pi (Figure 3C).
203 Similarly, Pi amounts also increased in Ubp3^{C469A} (Figure S3A). Therefore, the loss of Ubp3
204 increases intracellular Pi levels. Next, we asked if *ubp3Δ* cells exhibit signatures of a 'high Pi'
205 state. *S. cerevisiae* maintains internal Pi balance by controlling the expression of multiple
206 genes collectively known as the Pho regulon (41). The Pho regulon is induced under Pi
207 limitation, and repressed during Pi sufficiency (32, 41). We assessed two major Pho proteins
208 (Pho84: a high-affinity membrane Pi transporter, and Pho12: an acid phosphatase) in WT and
209 *ubp3Δ* in high glucose. *ubp3Δ* cells have lower amounts of Pho84 and Pho12 (Figure 3D).

210 Further, upon shifting to low Pi for one hour, Pho84 and Pho12 increased in *ubp3Δ*. These
211 data suggest that reduced Pho84 and Pho12 amounts in *ubp3Δ* are because of increased Pi,
212 and not due to altered Pho regulon function itself (Figure 3D). These data clarify earlier
213 observations from *ubp3Δ* which noted reduced Pho proteins (28). Therefore, *ubp3Δ*
214 constitutively have higher Pi, and likely a consequent decrease in Pho proteins.

215 We next asked if the increased Pi in *ubp3Δ* is because of altered G6P allocations
216 towards different end-points, particularly trehalose synthesis, which can be a major node of
217 Pi restoration (32, 35). We assessed the contribution of increased trehalose synthesis towards
218 the high Pi in *ubp3Δ*, by estimating Pi levels in the absence of trehalose 6-phosphate
219 phosphatase (Tps2), which catalyzes the Pi-releasing step in trehalose synthesis. Notably, loss
220 of Tps2 in *ubp3Δ* decreased Pi (Figure 3E). There was no additive difference in Pi between
221 *tps2Δ* and *ubp3Δtps2Δ* (Figure 3E). As an added control, we assessed trehalose in WT and
222 *ubp3Δ* in the absence of Tps2, and found no difference (Figure S3B). Therefore, increasing
223 G6P flux towards trehalose biosynthesis is a major source of the increased Pi in *ubp3Δ*.

224 Since the major GAPDH isozymes, Tdh2 and Tdh3, are reduced in *ubp3Δ*, we directly
225 asked if reducing GAPDH can decrease Pi consumption and increase Pi. To assess this, we
226 generated *tdh2Δtdh3Δ* cells, which exhibit a growth defect, but are viable, permitting further
227 analysis. *tdh2Δtdh3Δ* had higher Pi in high glucose (Figure 3F). Expectedly, we observed a
228 decrease in ethanol in *tdh2Δtdh3Δ* (Figure S3C), along with an accumulation of F1,6 BP and
229 G3P, and decreased 3PG and PEP (Figure S3D). However, G6P and trehalose levels between
230 WT and *tdh2Δtdh3Δ* were comparable (Figure S3D, S3E). These data sugest that unlike in
231 *ubp3Δ*, the increased Pi in *tdh2Δtdh3Δ* comes mainly from decreased Pi consumption (GAPDH
232 step). To further assess the role of reduced glycolytic flux in increasing Pi (*ubp3Δ* and
233 *tdh2Δtdh3Δ*), we measured the Pi in these cells growing in a gluconeogenic medium – 2%,
234 ethanol. In this scenario, the GAPDH catalyzed reaction will be reversed, converting 1,3BPG
235 to G3P, which should release and not consume Pi. Compared to WT, the Pi levels decreased
236 in *ubp3Δ* and *tdh2Δtdh3Δ* (Figure 3G), suggesting that the changes in Pi in these mutants is
237 driven by the relative change in Pi release vs consumption.

238 These results collectively indicate that the combined effect of increased Pi release
239 coming from trehalose synthesis, and decreased Pi consumption from reduced GAPDH
240 increase Pi levels in *ubp3Δ*.

241

242 **Mitochondrial Pi availability correlates with mitochondrial activity in *ubp3Δ***

243 We therefore wondered if this observed Pi increase from the combined rewiring of
244 glucose metabolism resulted in more Pi becoming accessible to the mitochondria. This would
245 effectively result in Pi budgeting between cytosolic glycolysis and mitochondria based on the
246 relative flux in different arms of glucose metabolism, by increasing Pi availability for the
247 mitochondria (Figure 4A). To test if this were so, we first asked if the mitochondria in *ubp3Δ*
248 have increased Pi. Mitochondria were isolated by immunoprecipitation from WT and *ubp3Δ*,
249 the isolation efficiency was analyzed (Figure S4A), and relative Pi levels compared. Pi levels
250 were normalised to Idh1 (isocitrate dehydrogenase) in isolated mitochondria, since Idh1
251 protein levels did not decrease in *ubp3Δ* (Figure S4B), and consistent with (28). Mitochondrial
252 Pi was higher in *ubp3Δ* (Figure 4B). We next asked if the increased mitochondrial activity in
253 *ubp3Δ* is a consequence of high Pi. If this were so, *tdh2Δtdh3Δ* should partially phenocopy
254 *ubp3Δ* with respect to mitochondrial activity. Consistently, *tdh2Δtdh3Δ* have higher
255 mitotracker intensity as well as Cox2 levels compared to WT (Figure S4C, Figure 4C). Also
256 consistent with this, a high basal OCR in *tdh2Δtdh3Δ* was observed (Figure 4D), together
257 indicating high mitochondrial activity in *tdh2Δtdh3Δ*, which is comparable to *ubp3Δ*.

258 We next asked if higher Pi is necessary to increase mitochondrial activity in *ubp3Δ* and
259 *tdh2Δtdh3Δ*. Since glycolysis is defective in *ubp3Δ* and *tdh2Δtdh3Δ*, it is necessary to
260 distinguish the effect of high Pi vs. only the effect of low glycolysis in activating mitochondria.
261 Logically, if decreased glycolysis (independent of Pi) is sufficient to activate mitochondria,
262 bringing down the Pi levels in *ubp3Δ* to that of WT should not affect mitochondrial activity.
263 Notably, *ubp3Δ* grown in low (1 mM) Pi have Pi levels similar to WT in standard (normal Pi)
264 medium (Figure S4D). *ubp3Δ* grown in low Pi also had decreased ethanol, suggesting reduced
265 glycolysis (Figure S4E). Therefore, we used this condition to further understand the role of Pi
266 in inducing mitochondrial activity. Mitotracker fluorescence decreased in both *ubp3Δ* and

267 *tdh2Δtdh3Δ* in low Pi (Figure S4F). Note: basal mitotracker fluorescence in WT also decreases
268 in low Pi, which is consistent with a required role of Pi for mitochondrial activity (Figure S4F).
269 Similarly, Cox2 levels were reduced in both *ubp3Δ* and *tdh2Δtdh3Δ* (Figure 4E). Consistent
270 with both reduced mitotracker intensity and Cox2 levels, basal OCR also decreased in both
271 *ubp3Δ* and *tdh2Δtdh3Δ* in low Pi (Figure 4F). These data collectively suggest that high
272 intracellular Pi is necessary to increase mitochondrial activity in *ubp3Δ* and *tdh2Δtdh3Δ*.

273 Next, we asked how mitochondrial Pi transport regulates mitochondrial activity. Mir1
274 and Pic2 are mitochondrial Pi transporters, with Mir1 being the major Pi transporter (42, 43).
275 We first limited mitochondrial Pi availability in *ubp3Δ* by knocking-out *MIR1*. In *mir1Δ*, the
276 increased Cox2 observed in *ubp3Δ* was no longer observed (Figure 4G). Consistent with this,
277 we observed no further increase in the basal OCR in *mir1Δubp3Δ* compared to *mir1Δ* (Figure
278 4H). Furthermore, *mir1Δ* showed decreased Cox2 as well as basal OCR even in WT cells (Figure
279 4G, Figure 4H). These data together suggest that mitochondrial Pi transport is critical for
280 increasing mitochondrial activity in *ubp3Δ*, and in maintaining basal mitochondrial activity
281 even in high glucose.

282 As a control, no significant increase in Mir1 and Pic2 was observed in *ubp3Δ* (Figure
283 S4G), suggesting that *ubp3Δ* do not increase mitochondrial Pi by merely increasing the Pi
284 transporters, but rather by increasing available Pi pools.

285 Taken together, these data suggest the possibility that increased cytosolic Pi increases
286 the mitochondrial Pi pool, which increases mitochondrial activity. Decreasing mitochondrial
287 Pi by either reducing total Pi, or by reducing mitochondrial Pi transport decreases
288 mitochondrial activity.

289

290 **Mitochondrial Pi availability constrains mitochondrial activity under high glucose**

291 So far, these data suggest that the cytosolic Pi available for the mitochondria can
292 dermine the extent of mitochondrial activity. Therefore, we further investigated if
293 mitochondrial Pi allocation was a necessary constraint for glucose-mediated mitochondrial
294 repression.

295 To test this, we first asked how important mitochondrial Pi transport was to switch to
296 increased respiration. In WT yeast, low glucose or glycolytic inhibition will result in increased
297 respiration (22). What happens therefore if we restrict mitochondrial Pi in this context? For
298 this, we measured the basal OCR in WT and *mir1Δ* after switching from high (2%) to low (0.1%)
299 glucose. We observed a significant increase in the basal OCR in WT but not in *mir1Δ* (Figure
300 5A). The alternate scenario is after glycolytic inhibition. We assessed the role of mitochondrial
301 Pi in this context, by inhibiting glycolysis using 2-deoxyglucose (2DG). WT, but not *mir1Δ*,
302 increased their OCR (respiration) upon a 1-hour treatment with 2DG (Figure 5B). Consistent
303 with this, mitotracker fluorescence increased with an increase in 2DG in WT, but not in *mir1Δ*
304 (Figure S5A). We further asked if the mitochondrial Pi transporter itself glucose repressed,
305 and therefore assessed Mir1 amounts in high and low glucose. Mir1 levels are higher upon a
306 shift to low glucose, and in cells grown in 2% ethanol, suggesting that Mir1 is glucose
307 repressed (Figure 5C, S5B). These data suggest that mitochondrial Pi transport is necessary
308 for increasing mitochondrial activity after glucose derepression.

309 We next asked whether just adding external Pi was sufficient to increase
310 mitochondrial activity, when cells are in high glucose. In medium supplemented with excess
311 Pi, the internal Pi increases as seen earlier (Figure 3C). Therefore, a simplistic assumption
312 would be that the addition of external Pi to cells in high glucose would also increase
313 mitochondrial Pi. However, an alternate possibility presents itself whererin since glycolytic
314 flux is already high in glucose, supplementing Pi will continue to fuel glycolysis. Indeed, this
315 was originally obseved by Harden and Young in 1908, where adding Pi increased fermentation
316 (44). In such a scenario, mitochondrial Pi will not increase. We estimated mitochondrial Pi in
317 this condition where excess Pi was externally supplemented. Notably, cells grown in high Pi
318 had decreased mitochondrial Pi (Figure S5C). Furthermore, directly adding Pi to cells growing
319 in high glucose decreased basal OCR (Figure S5D), consistent with decreased mitochondrial
320 Pi. These data indicate that in high glucose, simply supplementing Pi will not increase Pi access
321 to the mitochondria. We therefore now asked, if we inhibit glycolytic flux and then
322 supplement Pi, what would happen to mitochondrial activity. For this, we treated cells with
323 2DG, and subsequently added Pi and measured the OCR (Figure S5E). In this case,
324 supplementing Pi increased the basal OCR (Figure S5E). Collectively, these data suggest that
325 a combination of decreasing glycolysis and increasing Pi can together increase respiration.

326 Next, in order to directly test mitochondrial activation based on external Pi availability, we
327 isolated mitochondria, and estimated activity *in vitro* upon adding increasing Pi.
328 Mitochondrial activity increased with increased Pi, with maximum activity observed with 25
329 mM Pi supplemented (Figure 5D). In a complementary experiment, we overexpressed the
330 Mir1 transporter in wild-type cells, to increase Pi within mitochondria (Figure S5F). Mir1-OE
331 cells have higher Cox2 levels and basal OCR (Figure 5E, 5F). Therefore, increasing Pi transport
332 to mitochondria is sufficient to increase mitochondrial activity in high glucose.

333 Mitochondrial pyruvate transport is also required for mitochondrial respiration (45).
334 We asked where Pi availability stands in a hierarchy of constraints for mitochondrial
335 derepression, as compared to mitochondrial pyruvate transport. We measured the amounts
336 of the Mpc3 subunit of the mitochondrial pyruvate carrier (MPC) complex (45, 46). Mpc3
337 protein increases in *ubp3Δ* (Figure S5G), correlating with the increased mitochondrial activity.
338 Interestingly, in *ubp3Δ* grown in low Pi, Mpc3 further increased (Figure S5G), but as shown
339 earlier this condition cannot increase OCR or mitochondrial activity (Figure 4F, S4F). Basal
340 Mpc3 levels decrease in *mir1Δ*, but upon shifting to 0.1% glucose, Mpc3 increases in both WT
341 and *mir1Δ*, with higher levels in *mir1Δ* (Figure S5H). Therefore, even where Mpc3 is high
342 (*ubp3Δ* in low Pi, and *mir1Δ* in low glucose), mitochondrial activity remains low if Pi is
343 restricted (Figure 4F, 4H). There was also no decrease in basal OCR in *mpc3Δ* in high glucose,
344 and the basal OCR increased to the same level as of WT after shifting to 0.1% glucose (Figure
345 S5I). Since Mpc3 changes with mitochondrial Pi availability (Figure S5G, S5H), we also
346 measured Mpc3 in the Mir1OE. No further changes in Mpc3 were observed in Mir1OE (Figure
347 S5J), indicating that increasing mitochondrial Pi alone need not increase Mpc3. Overall,
348 although Mpc3 levels corelate with decreased glycolysis (*ubp3Δ* -Figure S5G, *ubp3Δ* in low Pi-
349 Figure S5G, low glucose -Figure S5H), increased Mpc3 alone cannot increase mitochondrial
350 activity and respiration in the absence of adequate mitochondrial Pi.

351 Finally, we asked how important mitochondrial Pi transport was for growth, under
352 2DG treatment. In the presence of 2DG, WT cells have only slightly decreased growth. In
353 contrast, *mir1Δ* show a severe growth defect upon 2DG treatment (Figure 5G), revealing a
354 synergetic effect of combining 2DG with inhibiting mitochondrial Pi transport. Therefore, the
355 combined inhibition of glycolysis and mitochondrial Pi transport restricts the growth of
356 glycolytic cells.

357 Collectively, mitochondrial Pi availability constrains glucose-mediated mitochondrial
358 repression. Increasing available pools of Pi to enter the mitochondria is sufficient to induce
359 mitochondrial activity.

360

361 **Discussion**

362 In this study, we highlight a role for Pi budgeting between cytosolic glycolysis and
363 mitochondrial processes (which compete for Pi) in constraining mitochondrial repression
364 (Figure 5H). Ubp3 controls this process (Figure 1), by maintaining the amounts of the glycolytic
365 enzymes Pfk1 and GAPDH (Tdh2 and Tdh3) and thereby allows high glycolytic flux. At high
366 fermentation rates, glycolytic enzymes levels at maximal activity maintain high glycolytic rates
367 (effectively following zero-order kinetics), and therefore, changes in the enzyme levels will
368 have a direct, proportionate effect on flux (47). The loss of Ubp3 decreases glycolytic flux,
369 resulting in a systems-level, mass-action based rewiring of glucose metabolism where more
370 G6P is routed towards trehalose synthesis and PPP (Figure 2, Figure 5H). Indeed, inhibiting
371 just phosphofructokinase can reroute glucose flux from glycolysis to PPP (48–50), and our
372 study now permits contextualized interpretations of these results. Such reallocations of
373 glucose flux will collectively increase overall Pi, coming from the combined effect of increased
374 Pi release from trehalose synthesis, and decreased Pi consumption via reduced GAPDH. This
375 altered intracellular Pi economy increases Pi pools available to mitochondria, and increasing
376 mitochondrial Pi is necessary and sufficient to increase respiration in high glucose (Figure 4,
377 Figure 5). Mitochondrial Pi transport maintains mitochondrial activity in high glucose, and
378 increases mitochondrial activity in low glucose (Figure 4, Figure 5). Finally, the mitochondrial
379 Pi transporter Mir1 itself decreases in high glucose (Figure 5). Therefore, this glucose-
380 dependent repression of Mir1 also restricts mitochondrial Pi availability (and thereby activity)
381 in high glucose.

382 Traditionally, loss-of-function mutants of metabolic enzymes are used to understand
383 metabolic state regulation. This approach negates nuanced investigations, since metabolic
384 enzymes are often essential for viability. Furthermore, metabolic pathways have multiple,
385 contextually regulated nodes, through which cells maintain their metabolic state. Therefore,

386 alternate approaches to identify global regulators of metabolic states (as opposed to single
387 enzymes), might uncover ways via which multiple nodes are simultaneously tuned, and can
388 reveal unanticipated systems-level principles of metabolic state rewiring. In this study of
389 glucose-mediated mitochondrial repression, the loss of the DUB Ubp3 decreases glycolytic
390 flux by reducing the enzymes at two critical nodes in the pathway - Pfk1 and GAPDH. Unlike
391 loss of function mutants, a reduction in amounts will only rewire metabolic flux. By 'hitting'
392 multiple steps in glycolysis simultaneously, *ubp3Δ* have decreased Pi consumption, as well as
393 increased Pi release. Such a cumulative phenomenon reveals more than inhibiting only
394 GAPDH, where increased Pi comes only from reduced Pi consumption, and not from increased
395 trehalose biosynthesis. Our serendipitous identification of a regulator which regulates
396 multiple steps in glucose metabolism to change the metabolic environment, now suggests a
397 general basis of mitochondrial regulation that would have otherwise remained hidden.
398 Separately, finding the substrates of Ubp3 and whether Ubp3 directly regulates glycolytic
399 enzymes are exciting future research questions requiring concurrent innovations in accessible
400 chemical-biological approaches to study DUBs.

401 Because phosphates are ubiquitous, it is challenging to identify hierarchies of Pi-
402 dependent processes in metabolic state regulation (33). Phosphate transfer reactions are the
403 foundation of metabolism, driving multiple, thermodynamically unfavorable reactions (51,
404 52). Contextually, the laws of mass action predict that the relative rates of these reactions will
405 regulate overall Pi balance, and contrarily the Pi allocation to Pi-dependent reactions will
406 determine reaction rates (33, 35). Additionally, cells might control Pi allocations for different
407 reactions via compartmentalizing Pi in organelles, to spatially restrict Pi availability (53–55).
408 Our data collectively suggest a paradigm where the combination of factors regulates
409 mitochondrial Pi and thereby activity. In glycolytic yeast cells growing in high glucose,
410 mitochondrial Pi availability becomes restricted due to higher utilization of Pi in glycolysis
411 compared to mitochondria. Consistent with this, a rapid decrease in Pi upon glucose addition
412 has been observed (18, 19, 37). Interesting, *in vitro* studies with isolated mitochondria from
413 tumor cells also find that decreasing Pi levels decreases respiration (19), which would be
414 consistent with this scenario. Further, supplementing Pi correlates with decreased
415 mitochondrial repression in tumors (18, 56). By increasing Pi through a systems-level rewiring
416 of glucose metabolism (such as in *ubp3Δ* cells), cells can collectively increase mitochondrial

417 access to Pi. This Pi budgeting determines mitochondrial activity. Supplementing Pi under
418 conditions of low glycolysis (where mitochondrial Pi transport is enhanced), as well as directly
419 supplementing Pi to isolated mitochondria, increases respiration (Figure 5, S5). Therefore, in
420 order to deprepress mitochondria, a combination of increased Pi along with decreased
421 glycolysis is required. An additional systems-level phenomenon that might regulate Pi
422 transport to the mitochondria is the decrease in cytosolic pH upon decreased glycolysis (57,
423 58). Since mitochondrial Pi transport itself dependeds on the proton gradient, a low cytosolic
424 pH would favour mitochondrial Pi transport (59). Therefore, decreasing glycolysis (2DG
425 treatment, deletion of Ubp3, and decreased GAPDH activity), and increasing cytosolic Pi might
426 synergestically increase mitochondria Pi transport, and increase respiration. Alternately,
427 increasing mitochondrial Pi transporter amounts can achieve the same result, as seen by
428 overexpressing Mir1 (Figure 5). A similar observation has been reported in *Arabidopsis*,
429 reiterating an evolutionarily conserved role for mitochondrial Pi in controlling respiration
430 (60). Relatedly, glycolytic inhibition can suppress cell proliferation in Warburg-positive tumors
431 (61, 62), or inflammatory responses (63). However, these cells survive by switching to
432 mitochondrial respiration (64, 65), requiring alternate approaches to prevent their
433 proliferation (66). Inhibiting mitochondrial Pi transport in combination with glycolytic
434 inhibition could restrict the proliferation of Warburg/Crabtree positive cells.

435 Since its discovery in the 1920s, the phenomenon of accelerated glycolysis with
436 concurrent mitochondrial repression has been intensely researched. Yet, the biochemical
437 constraints for glucose-mediated mitochondrial repression remains unresolved. One
438 hypothesis suggests that the availability of glycolytic intermediates might determine the
439 extent of mitochondrial repression. F1,6BP inhibits complex III and IV of the electron transport
440 chain (ETC) in Crabtree positive yeast (14–17). Similarly, the ratio between G6P and F1,6BP
441 regulates the extent of mitochondrial repression (16, 17). Although G6P/F6P accumulates in
442 *ubp3Δ* (Figure 2C), this is not the case in *tdh2Δtdh3Δ* (GAPDH mutant) (Figure S3D), suggesting
443 that G6P/F6P accumulation in itself is not the criterion to increase mitochondrial activity.
444 Separately, the competition for common metabolites/co-factors between glycolysis and
445 respiration (such as ADP, Pi or pyruvate) could drive this phenomenon (14, 18). Here we
446 observe that Mpc3 mediated mitochondrial pyruvate transport alone cannot increase
447 respiration. An additional consideration is the possible contribution of changes in ADP in

448 regulating mitochondrial activity, where the use of ADP in glycolysis might limit mitochondrial
449 ADP. Therefore, when Pi changes as a consequence of glycolysis, it coud be imagined that a
450 change in ADP balance can coincidentally occur. However, prior studies show that even
451 though cytosolic ADP decreases in the presence of glucose, this does not limit mitochondrial
452 ADP uptake, or decrease respiration, due to the very high affinity of the mitochondrial ADP
453 transporter (14, 19). These collectively reiterate the importance of Pi access and transport to
454 mitochondria in constraining mitochondrial respiration. Indeed, this interpretation can also
455 contextually explain observations from other model systems where mitochondrial Pi
456 transport seems to regulate respiration (67, 68).

457 We parsimoniously suggest that Pi access to the mitochondria as a key constraint for
458 mitochondrial repression under high glucose. In a hypothetical scenario, a single-step event
459 in evolution, reducing mitochondrial Pi transporter amounts, and/or increasing glycolytic flux
460 (to deplete cytosolic Pi), will result in whole-scale metabolic rewiring to repress mitochondria.
461 More elaborate regulatory events can easily be imagined as subsequent adaptations to
462 enforce mitochondrial repression. Given the central role played by Pi, something as
463 fundamental as access to Pi will constrain mitochondrial repression. Concurrently, the rapid
464 incorporation of Pi into faster glycolysis can give cells a competitive advantage, while also
465 sequestering Pi in the form of usable ATP. Over the course of evolution, this could conceivably
466 drive other regulatory mechanisms to enforce mitochondrial repression, leading to the
467 currently observed complex regulatory networks and signaling programs observed in the
468 Crabtree effect, and other examples of glucose-dependent mitochondrial repression.

469

470 ## Materials and methods

471 ### Statistics and graphing

472 Unless otherwise indicated, statistical significance for all indicated experiments were
473 calculated using unpaired Student's t-tests (GraphPad prism 9.0.1). Graphs were plotted using
474 GraphPad prism 9.0.1

475 ### Yeast strains, media, and growth conditions

476 A prototrophic CEN.PK strain of *Saccharomyces cerevisiae* (WT) (69) was used. Strains are
477 listed in appendix table S1. Gene deletions, chromosomal C-terminal tagged strains were
478 generated by PCR mediated gene deletion/tagging (70). Media compositions, growth
479 conditions and CRISPR-Cas9 based mutagenesis are described in extended methods (SI
480 appendix).

481 **Mitotracker fluorescence**

482 Mitotracker fluorescence was measured using Thermo Varioscan™ LUX multimode plate
483 reader (579/599 excitation/emission). Detailed protocol is described in extended methods.
484 Mitotracker fluorescence were normalized using OD_{600} of each sample and relative
485 fluorescence intensity calculated.

486 **Protein extraction and Western blotting**

487 Total protein was precipitated, extracted using trichloroacetic acid (TCA) as described earlier
488 (71). Blots were quantified using ImageJ software. Detailed protocol is described in extended
489 methods.

490 **Basal OCR measurement**

491 The basal OCR was measured using Agilent Seahorse XFe24 analyzer. Basal OCR readings were
492 normalized for cell number (using OD_{600} of samples) in each well. The detailed methods are
493 described in extended methods.

494 **RNA extraction and RT-qPCR**

495 The RNA extraction was done using the hot phenol extraction method as described in (71).
496 The isolated RNA was DNase treated, and used for cDNA synthesis. Superscript III reverse
497 transcriptase enzyme (Invitrogen) was used for cDNA synthesis and RT-qPCR was performed
498 using KAPA SYBR FAST qRT PCR kit (KK4602, KAPA Biosystems). Taf10 was used as a control
499 for normalisation and the fold change in mRNA levels were calculated by 2^-ddct method.

500 **ATP, ethanol and Pi measurements**

501 ATP levels were measured by ATP estimation kit (Thermo Fisher A22066). Ethanol
502 concentration in the medium was estimated using potassium dichromate based assay
503 described in (72) with modifications. Pi was estimated using a malachite green phosphate
504 assay kit (Cayman chemicals, 10009325). Detailed sample collection and assay protocols are
505 described in extended methods.

506 **Metabolite extraction and analysis by LC-MS/MS**

507 The steady state levels and relative ^{13}C label incorporation into metabolites were estimated
508 by quantitative LC-MS/MS methods as described in (73). Detailed methodology is extensively
509 described in extended methods. Peak area measurements are listed in supplement file 1.

510 **Mitochondrial isolation**

511 Mitochondria was isolated by immunoprecipitation as described in (74, 75) with
512 modifications. The detailed protocol is described in extended methods (SI appendix). The
513 eluted mitochondria were used in malachite green assay for Pi estimation, boiled with SDS-
514 glycerol buffer for western blots or incubated with mitotracker CMXROS with mitochondria-
515 activation buffer for mitotracker assays.

516

517 ## Data availability

518 The LC-MS/MS peak area for all the metabolites can be found in supplement file 1. This study
519 includes no data deposited in external repositories.

520

521 ## Acknowledgements

522 We thank all SL lab members, Benjamin Tu, Anand Bachhawat and Vijay Jayaraman for
523 comments and suggestions. We acknowledge the NCBS/inStem/CCAMP mass spectrometry
524 facility for LC-MS/MS support. We thank Aayushee Khanna for help with experiments. V.V
525 acknowledges funding support from DST-INSPIRE fellowship (IF170236) from the Department
526 of Science and Technology (DST), Govt. of India, S.N and SA acknowledges intramural funding

527 from the DBT-inStem PhD program. S.L acknowledges support from the DST SERB CRG grant
528 CRG/2019/004772, a DBT-Wellcome India Alliance Senior Fellowship (IA/S/21/2/505922), and
529 institutional support from inStem.

530 **References**

531 1. J. Zhu, C. B. Thompson, Metabolic regulation of cell growth and proliferation. *Nat.*
532 *Rev. Mol. Cell Biol.* **20**, 436–450 (2019).
533 2. L. Cai, B. P. Tu, Driving the Cell Cycle Through Metabolism. *Annu. Rev. Cell Dev. Biol.*
534 **28**, 59–87 (2011).
535 3. D. L. (David L. Nelson, D. L. (David L. Nelson, A. L. Lehninger, M. M. Cox, Lehninger
536 principles of biochemistry (2008) (March 10, 2022).
537 4. O. Warburg, The metabolism of carcinoma cells 1. *J. Cancer Res.* **9**, 148–163 (1925).
538 5. M. G. Vander Heiden, L. C. Cantley, C. B. Thompson, Understanding the Warburg
539 Effect: The Metabolic Requirements of Cell Proliferation. *Science (80-.).* **324**, 1029–
540 1033 (2009).
541 6. H. G. Crabtree, Observations on the carbohydrate metabolism of tumours. *Biochem.*
542 *J.* **23**, 536–545 (1929).
543 7. R. H. De Deken, The Crabtree effect: a regulatory system in yeast. *J. Gen. Microbiol.*
544 **44**, 149–156 (1966).
545 8. L. Xia, *et al.*, The cancer metabolic reprogramming and immune response. *Mol.*
546 *Cancer* **20**, 1–21 (2021).
547 9. M. D. Kornberg, The immunologic Warburg effect: Evidence and therapeutic
548 opportunities in autoimmunity. *Wiley Interdiscip. Rev. Syst. Biol. Med.* **12**, 1–17
549 (2020).
550 10. N. Pacini, F. Borziani, Cancer stem cell theory and the warburg effect, two sides of the
551 same Coin? *Int. J. Mol. Sci.* **15**, 8893–8930 (2014).
552 11. A. M. Abdel-Haleem, *et al.*, The emerging facets of non-cancerous Warburg effect.
553 *Front. Endocrinol. (Lausanne).* **8**, 1–7 (2017).
554 12. E. Tsogtbaatar, C. Landin, K. Minter-Dykhouse, C. D. L. Folmes, Energy Metabolism
555 Regulates Stem Cell Pluripotency. *Front. Cell Dev. Biol.* **8**, 1–16 (2020).
556 13. A. Cornish-Bowden, Biochemical evolution : the pursuit of perfection. *Garl. Sci.*
557 (2016).

558 14. R. Diaz-Ruiz, M. Rigoulet, A. Devin, The Warburg and Crabtree effects: On the origin
559 of cancer cell energy metabolism and of yeast glucose repression. *Biochim. Biophys.*
560 *Acta - Bioenerg.* **1807**, 568–576 (2011).
561 15. N. Hammad, M. Rosas-Lemus, S. Uribe-Carvajal, M. Rigoulet, A. Devin, The Crabtree
562 and Warburg effects: Do metabolite-induced regulations participate in their
563 induction? *Biochim. Biophys. Acta - Bioenerg.* **1857**, 1139–1146 (2016).
564 16. R. Díaz-Ruiz, *et al.*, Mitochondrial Oxidative Phosphorylation Is Regulated by Fructose
565 1,6-Bisphosphate: A POSSIBLE ROLE IN CRABTREE EFFECT INDUCTION? *. *J. Biol.*
566 *Chem.* **283**, 26948–26955 (2008).
567 17. M. R. Lemus, *et al.*, The role of glycolysis-derived hexose phosphates in the induction
568 of the Crabtree effect. *J. Biol. Chem.* **293**, 12843–12854 (2018).
569 18. D. H. Koobs, Phosphate mediation of the Crabtree and Pasteur effects. *Science (80-.).*
570 **178**, 127–133 (1972).
571 19. S. Rodríguez-Enríquez, O. Juárez, J. S. Rodríguez-Zavala, R. Moreno-Sánchez, Multisite
572 control of the Crabtree effect in ascites hepatoma cells. *Eur. J. Biochem.* **268**, 2512–
573 2519 (2001).
574 20. F. Tripodi, R. Nicastro, V. Reghellin, P. Coccetti, Post-translational modifications on
575 yeast carbon metabolism: Regulatory mechanisms beyond transcriptional control.
576 *Biochim. Biophys. Acta - Gen. Subj.* **1850**, 620–627 (2015).
577 21. T. Hitosugi, J. Chen, Post-translational modifications and the Warburg effect.
578 *Oncogene* **33**, 4279–4285 (2014).
579 22. J. R. Broach, Nutritional control of growth and development in yeast. *Genetics* **192**,
580 73–105 (2012).
581 23. A. Hershko, A. Ciechanover, THE UBIQUITIN SYSTEM. *Annu. Rev. Biochem.* **67**, 425–79
582 (1998).
583 24. D. Komander, M. Rape, The Ubiquitin Code. *Annu. Rev. Biochem.* **81**, 203–229 (2012).
584 25. C. M. Pickart, M. J. Eddins, Ubiquitin: Structures, functions, mechanisms. *Biochim.*
585 *Biophys. Acta - Mol. Cell Res.* **1695**, 55–72 (2004).
586 26. E. Postma, C. Verduyn, W. A. Scheffers, J. P. Van Dijken, Enzymic analysis of the
587 crabtree effect in glucose-limited chemostat cultures of Saccharomyces cerevisiae.
588 *Appl. Environ. Microbiol.* **55**, 468–77 (1989).
589 27. B. Ossareh-Nazari, *et al.*, Cdc48 and Ufd3, new partners of the ubiquitin protease

590 Ubp3, are required for ribophagy. *EMBO Rep.* **11**, 548–554 (2010).
591 28. M. Isasa, *et al.*, Multiplexed, Proteome-Wide Protein Expression Profiling: Yeast
592 Deubiquitylating Enzyme Knockout Strains. *J. Proteome Res.* **14**, 5306–5317 (2015).
593 29. R. Nostramo, S. N. Varia, B. Zhang, M. M. Emerson, P. K. Herman, The Catalytic
594 Activity of the Ubp3 Deubiquitinating Protease Is Required for Efficient Stress Granule
595 Assembly in Saccharomyces cerevisiae. *Mol. Cell. Biol.* **36**, 173 (2016).
596 30. F. Fontanesi, I. C. Soto, D. Horn, A. Barrientos, Assembly of mitochondrial cytochrome
597 c-oxidase, a complicated and highly regulated cellular process. *Am. J. Physiol. - Cell*
598 *Physiol.* **291**, 1129–1147 (2006).
599 31. A. A. Shestov, *et al.*, Quantitative determinants of aerobic glycolysis identify flux
600 through the enzyme GAPDH as a limiting step. *Elife* **3**, 1–18 (2014).
601 32. R. Gupta, *et al.*, A tRNA modification balances carbon and nitrogen metabolism by
602 regulating phosphate homeostasis. *Elife* **8**, 1–33 (2019).
603 33. R. Gupta, S. Laxman, Cycles, sources, and sinks: Conceptualizing how phosphate
604 balance modulates carbon flux using yeast metabolic networks. *Elife* **10**, 1–14 (2021).
605 34. P. W. Mason, D. P. Carbone, R. A. Cushman, A. S. Waggoner, The importance of
606 inorganic phosphate in regulation of energy metabolism of Streptococcus lactis. *J.*
607 *Biol. Chem.* **256**, 1861–1866 (1981).
608 35. J. H. Van Heerden, *et al.*, Lost in transition: Start-up of glycolysis yields subpopulations
609 of nongrowing cells. *Science (80-.).* **343** (2014).
610 36. P. C. Brazy, L. J. Mandel, V. W. Dennis, S. R. Gullans, Metabolic Requirement for
611 Inorganic Phosphate by the Rabbit Proximal Tubule: EVIDENCE FOR A CRABTREE
612 EFFECT Metabolic Requirement for Inorganic Phosphate by the Rabbit Proximal
613 Tubule EVIDENCE FOR A CRABTREE EFFECT. *J Clin Invest* **70**, 53 (1982).
614 37. S. Hohmann, W. Bell, M. J. Neves, D. Valckx, J. M. Thevelein, Evidence for trehalose-6-
615 phosphate-dependent and-independent mechanisms in the control of sugar influx
616 into yeast glycolysis. *Mol. Microbiol.* **20**, 981–991 (1996).
617 38. T. Hunter, Why nature chose phosphate to modify proteins. *Philos. Trans. R. Soc. B*
618 *Biol. Sci.* **367**, 2513–2516 (2012).
619 39. P. O. Ljungdahl, B. Daignan-Fornier, Regulation of amino acid, nucleotide, and
620 phosphate metabolism in Saccharomyces cerevisiae. *Genetics* **190**, 885–929 (2012).
621 40. S. Austin, A. Mayer, Phosphate Homeostasis − A Vital Metabolic Equilibrium

622 Maintained Through the INPHORS Signaling Pathway. *Front. Microbiol.* **11**, 1367
623 (2020).
624 41. J. M. Mouillon, B. L. Persson, New aspects on phosphate sensing and signalling in
625 Saccharomyces cerevisiae. *FEMS Yeast Res.* **6**, 171–176 (2006).
626 42. H. Murakami, G. Blobel, D. Pain, Isolation and characterization of the gene for a yeast
627 mitochondrial import receptor. *Nat. 1990 3476292* **347**, 488–491 (1990).
628 43. V. Zara, *et al.*, Yeast mitochondria lacking the phosphate carrier/p32 are blocked in
629 phosphate transport but can import preproteins after regeneration of a membrane
630 potential. *Mol. Cell. Biol.* **16**, 6524–6531 (1996).
631 44. A. Harden, W. J. Young, The alcoholic Ferment of Yeast-juice.Part III.-The Function of
632 Phosphates in the Fermentation o f Glucose hy Yeast-juice. *Proc. R. Soc. London. Ser.*
633 *B,* **80**, 299–311 (1908).
634 45. A. Timoń-Gómez, M. Proft, A. Pascual-Ahuir, Differential Regulation of Mitochondrial
635 Pyruvate Carrier Genes Modulates Respiratory Capacity and Stress Tolerance in Yeast.
636 *PLoS One* **8**, e79405 (2013).
637 46. T. Bender, G. Pena, J.-C. Martinou, Regulation of mitochondrial pyruvate uptake by
638 alternative pyruvate carrier complexes. *EMBO J.* **34**, 911–924 (2015).
639 47. P. Grigaitis, B. Teusink, An excess of glycolytic enzymes under glucose-limited
640 conditions may enable Saccharomyces cerevisiae to adapt to nutrient availability.
641 *FEBS Lett.* (2022) https:/doi.org/10.1002/1873-3468.14484 (November 28, 2022).
642 48. W. Yi, *et al.*, PFK1 Glycosylation Is a Key Regulator of Cancer Cell Growth and Central
643 Metabolic Pathways. *Science* **337**, 975 (2012).
644 49. H. Miyazawa, *et al.*, Rewiring of embryonic glucose metabolism via suppression of
645 PFK-1 and aldolase during mouse chorioallantoic branching. *Dev.* **144**, 63–73 (2017).
646 50. W. D. Hollinshead, *et al.*, Examining Escherichia coli glycolytic pathways, catabolite
647 repression, and metabolite channeling using Δpfk mutants. *Biotechnol. Biofuels* **9**, 1–
648 13 (2016).
649 51. F. H. Westheimer, Why Nature Chose Phosphates. *Science (80-.).* **235**, 1173–1178
650 (1987).
651 52. S. C. L. Kamerlin, P. K. Sharma, R. B. Prasad, A. Warshel, Why nature really chose
652 phosphate. *Q. Rev. Biophys.* **46**, 1–132 (2013).
653 53. J. W. Booth, G. Guidotti, Phosphate Transport in Yeast Vacuoles *. *J. Biol. Chem.* **272**,

654 20408–20413 (1997).
655 54. T. Vila, S. Frases, F. M. Gomesid, Lessons from protozoans: Phosphate sensing and
656 polyphosphate storage in fungi. *PLOS Pathog.* **18**, e1010298 (2022).
657 55. M. E. Solesio, *et al.*, Depletion of mitochondrial inorganic polyphosphate (polyP) in
658 mammalian cells causes metabolic shift from oxidative phosphorylation to glycolysis.
659 *Biochem. J.* **478**, 1631–1646 (2021).
660 56. M. Brin, R. W. McKee, The Inhibition of Respiration by Glucose, Fructose, and
661 Mannose in the Ehrlich Mouse Ascites Tumor. *Cancer Res.* **16**, 364–368 (1956).
662 57. R. Orij, S. Brul, G. J. Smits, Intracellular pH is a tightly controlled signal in yeast.
663 *Biochim. Biophys. Acta - Gen. Subj.* **1810**, 933–944 (2011).
664 58. R. Dechant, *et al.*, Cytosolic pH is a second messenger for glucose and regulates the
665 PKA pathway through V-ATPase. *EMBO J.* **29**, 2515–2526 (2010).
666 59. P. Hamel, *et al.*, Redundancy in the function of mitochondrial phosphate transport in
667 Saccharomyces cerevisiae and Arabidopsis thaliana. *Mol. Microbiol.* **51**, 307–317
668 (2004).
669 60. F. Jia, *et al.*, Overexpression of Mitochondrial Phosphate Transporter 3 Severely
670 Hampers Plant Development through Regulating Mitochondrial Function in
671 Arabidopsis. *PLoS One* **10**, e0129717 (2015).
672 61. H. Pelicano, D. S. Martin, R. Xu, P. Huang, Glycolysis inhibition for anticancer
673 treatment. 4633–4646 (2006).
674 62. S. O'Neill, R. K. Porter, N. McNamee, V. G. Martinez, L. O'Driscoll, 2-Deoxy-D-Glucose
675 inhibits aggressive triple-negative breast cancer cells by targeting glycolysis and the
676 cancer stem cell phenotype. *Sci. Rep.* **9**, 1–11 (2019).
677 63. G. Soto-Heredero, M. M. Gómez de las Heras, E. Gabandé-Rodríguez, J. Oller, M.
678 Mittelbrunn, Glycolysis – a key player in the inflammatory response. *FEBS J.* **287**,
679 3350–3369 (2020).
680 64. R. Shiratori, *et al.*, Glycolytic suppression dramatically changes the intracellular
681 metabolic profile of multiple cancer cell lines in a mitochondrial metabolism-
682 dependent manner. *Sci. Rep.* **9**, 1–15 (2019).
683 65. C. L. Lu, *et al.*, Tumor Cells Switch to Mitochondrial Oxidative Phosphorylation under
684 Radiation via mTOR-Mediated Hexokinase II Inhibition - A Warburg-Reversing Effect.
685 *PLoS One* **10**, e0121046 (2015).

686 66. G. Cheng, *et al.*, Mitochondria-targeted drugs synergize with 2-deoxyglucose to
687 trigger breast cancer cell death. *Cancer Res.* **72**, 2634–2644 (2012).
688 67. M. Scheibye-Knudsen, B. Quistorff, Regulation of mitochondrial respiration by
689 inorganic phosphate; comparing permeabilized muscle fibers and isolated
690 mitochondria prepared from type-1 and type-2 rat skeletal muscle. *Eur. J. Appl.*
691 *Physiol.* **105**, 279–287 (2009).
692 68. E. L. Seifert, E. Ligeti, J. A. Mayr, N. Sondheimer, G. Hajnóczky, The mitochondrial
693 phosphate carrier: Role in oxidative metabolism, calcium handling and mitochondrial
694 disease. *Biochem. Biophys. Res. Commun.* **464**, 369–375 (2015).
695 69. J. B. J.P. van Dijken, *et al.*, An interlaboratory comparison of physiological and genetic
696 properties of four Saccharomyces cerevisiae strains. *Enzyme Microb. Technol.* **26**,
697 706–714 (2000).
698 70. M. S. Longtine, *et al.*, Additional modules for versatile and economical PCR-based
699 gene deletion and modification in Saccharomyces cerevisiae. *Yeast* **14**, 953–961
700 (1998).
701 71. V. Vengayil, Z. Rashida, S. Laxman, The E3 ubiquitin ligase Pib1 regulates effective
702 gluconeogenic shutdown upon glucose availability. *J. Biol. Chem.* **294**, 17209–17223
703 (2019).
704 72. M. Sriariyanun, P. Mutrakulcharoen, S. Tepaamorndech, K. Cheenkachorn, K.
705 Rattanaporn, A Rapid Spectrophotometric Method for Quantitative Determination of
706 Ethanol in Fermentation Products. *Orient. J. Chem.* **35**, 744–750 (2019).
707 73. A. Walvekar, Z. Rashida, H. Maddali, S. Laxman, A versatile LC-MS / MS approach for
708 comprehensive , quantitative analysis of central metabolic pathways [version 1 ; peer
709 review : 2 approved]. 1–15 (2018).
710 74. P. C. Liao, I. R. Boldogh, S. E. Siegmund, Z. Freyberg, L. A. Pon, Isolation of
711 mitochondria from Saccharomyces cerevisiae using magnetic bead affinity
712 purification. *PLoS One* **13**, 1–15 (2018).
713 75. W. W. Chen, E. Freinkman, D. M. Sabatini, Rapid immunopurification of mitochondria
714 for metabolite profiling and absolute quantification of matrix metabolites. *Nat.*
715 *Protoc.* **12**, 2215 (2017).
716
717

Figure 1: A deubiquitinase deletion screen identifies Ubp3 as a regulator of glucose-mediated mitochondrial repression

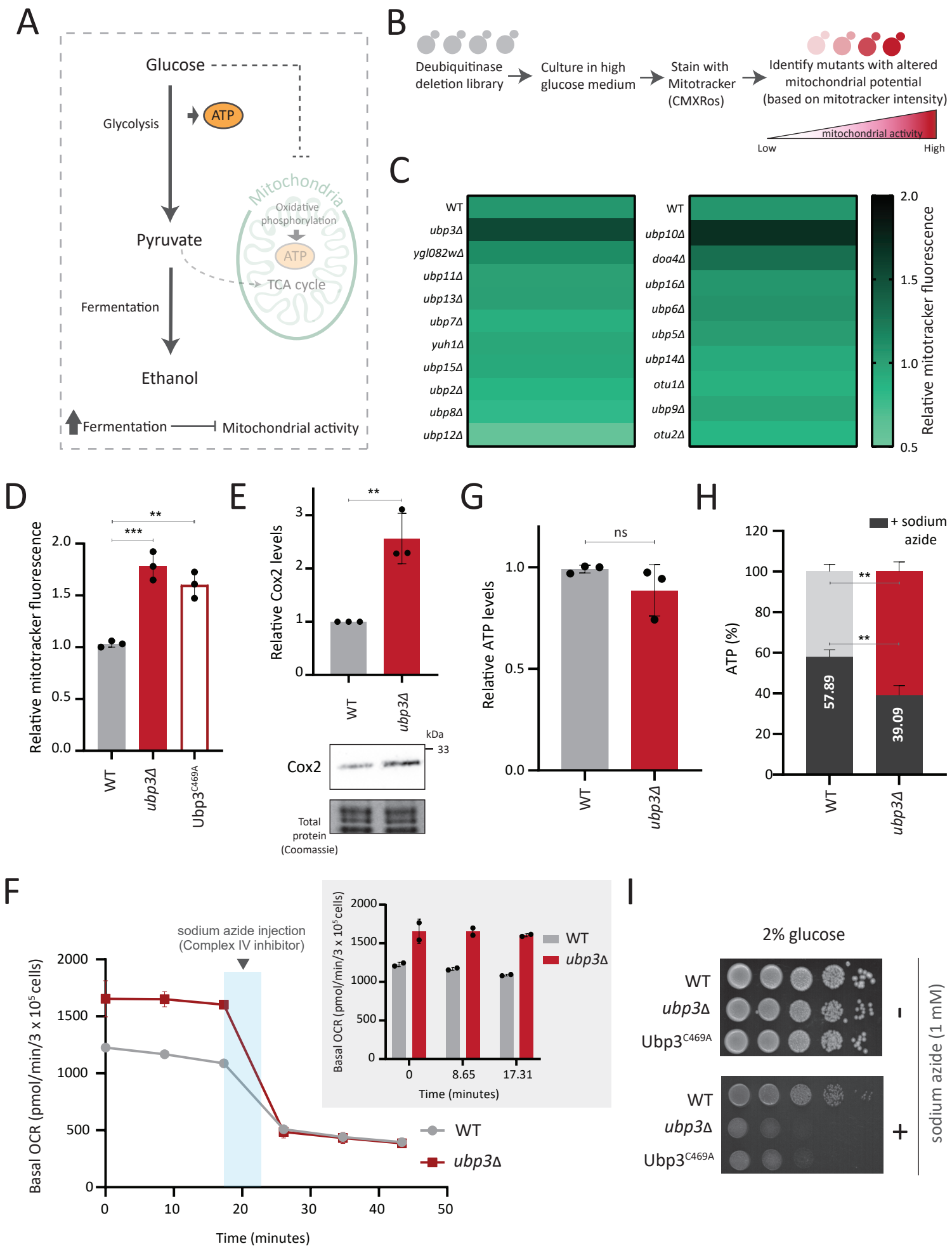

Figure 1: A deubiquitinase deletion screen identifies Ubp3 as a regulator of glucose-mediated mitochondrial repression

A) Schematic depicting glucose-mediated mitochondrial repression (Crabtree effect).

B) Schematic describing the screen with a yeast DUB KO library to identify regulators of Crabtree effect.

C) Identifying DUB knockouts with altered mitochondrial potential. Heat map shows relative mitochondrial membrane potential of 19 deubiquitinase deletions in high glucose, from 2 biological replicates. Also see figures S1A, S1B.

D) The deubiquitinase activity of Ubp3 and repression of mitochondrial membrane potential. WT, *ubp3Δ,* and Ubp3^{C469A} were grown in high glucose and relative mitochondrial membrane potential was measured. Data represent mean ± SD from three biological replicates (n=3). Also see figure S1D.

E) Effect of loss of Ubp3 on ETC complex IV subunit Cox2. WT and *ubp3Δ* were grown in high glucose, and Cox2 was measured (western blot using an anti-Cox2 antibody). A representative blot (out of 3 biological replicates, n=3) and their quantifications are shown. Data represent mean ± SD.

F) Basal oxygen consumption rate (OCR) in high glucose in *ubp3Δ*. WT and *ubp3Δ* were grown in high glucose, and OCR was measured. Basal OCR corresponding to ~3 x 10^5 cells, from two independent experiments (n=2), normalized to the OD_{600} is shown. Bar graph representations are shown in the inset. Data represent mean ± SD.

G) Total ATP levels in *ubp3Δ* and WT. WT and *ubp3Δ* were grown in high glucose, and total ATP were measured. Data represent mean ± SD from three biological replicates (n=3).

H) Dependence of *ubp3Δ* on mitochondrial ATP. WT and *ubp3Δ* cells were grown in high glucose, and treated with 1 mM sodium azide for 45 minutes. Total ATP levels in sodium azide treated and untreated cells were measured. Data represent mean ± SD (n=3).

I) Requirement for mitochondrial respiration in high glucose in *ubp3Δ*. Serial dilution growth assay in high glucose in the presence/absence of sodium azide (1 mM) are shown. Also see figure S1F.

Data information: **p<0.01, ***p<0.001.

Figure 2: Key glycolytic enzymes decrease and glucose flux is rerouted in *ubp3Δ* cells

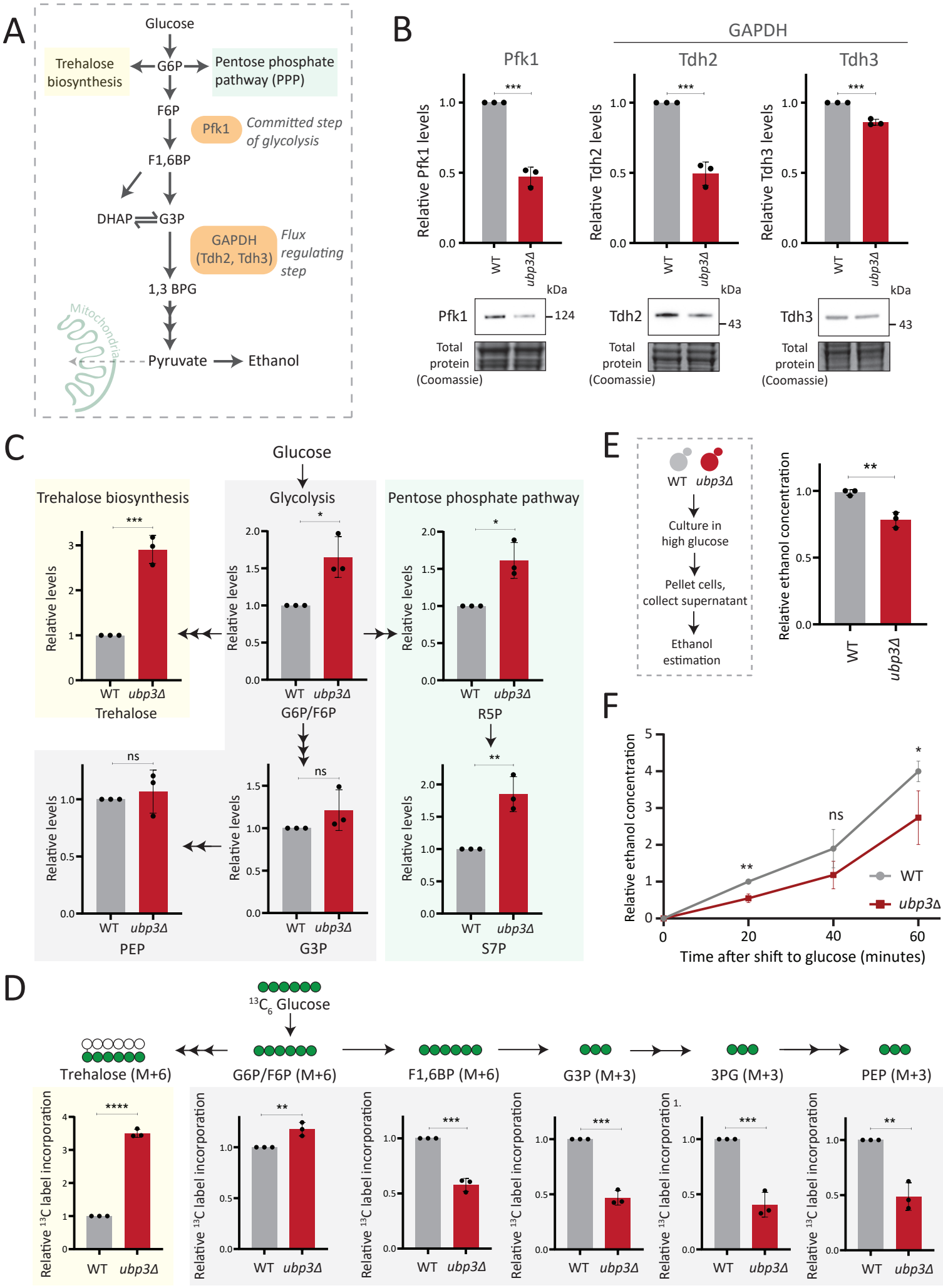

Figure 2: Key glycolytic enzymes decrease and glucose flux is rerouted in *ubp3Δ* cells

A) A schematic illustrating directions of glucose-6-phosphate (G6) flux in cells. Glucose is converted to G6P, a precursor for trehalose, the pentose phosphate pathway (PPP), and glycolysis.

B) Effect of loss of Ubp3 on key glycolytic enzymes. WT and *ubp3Δ* were grown in high glucose and the Pfk1, Tdh2, and Tdh3 levels were measured by western blot using an anti-FLAG antibody. A representative blot (out of three biological replicates, n=3) and their quantification are shown. Data represent mean ± SD. Also see figure S2A.

C) Steady-state metabolite amounts in WT and *ubp3Δ* in high glucose. Relative steady-state levels of trehalose, major glycolytic, and PPP intermediates were estimated in WT and *ubp3Δ*. Data represent mean ± SD from three biological replicates (n=3). Also see Appendix Table S3.

D) Relative glycolytic and trehalose synthesis flux in WT and *ubp3Δ*. Relative ^{13}C-label incorporation into trehalose and glycolytic intermediates, after a pulse of 1% $^{13}C_6$ glucose is shown. Data represent mean ± SD from three biological replicates (n=3). Also see Appendix Table S3, figures S2B, S2C.

E) Ethanol production in *ubp3Δ*. WT and *ubp3Δ* were grown in high glucose and ethanol in the media was measured. Data represent mean ± SD from three biological replicates (n=3).

F) Relative rate of ethanol production in WT vs *ubp3Δ*. WT and *ubp3Δ* were grown in high glucose (to OD_{600} ~ 0.6), equal numbers of cells were shifted to fresh medium (high glucose) and ethanol concentration in the medium was measured temporally. Data represent mean ± SD from three biological replicates (n=3)

Data information: *p<0.05, **p<0.01, ***p<0.001.

Figure 3: Rerouted glucose flux results in phosphate (Pi) accumulation

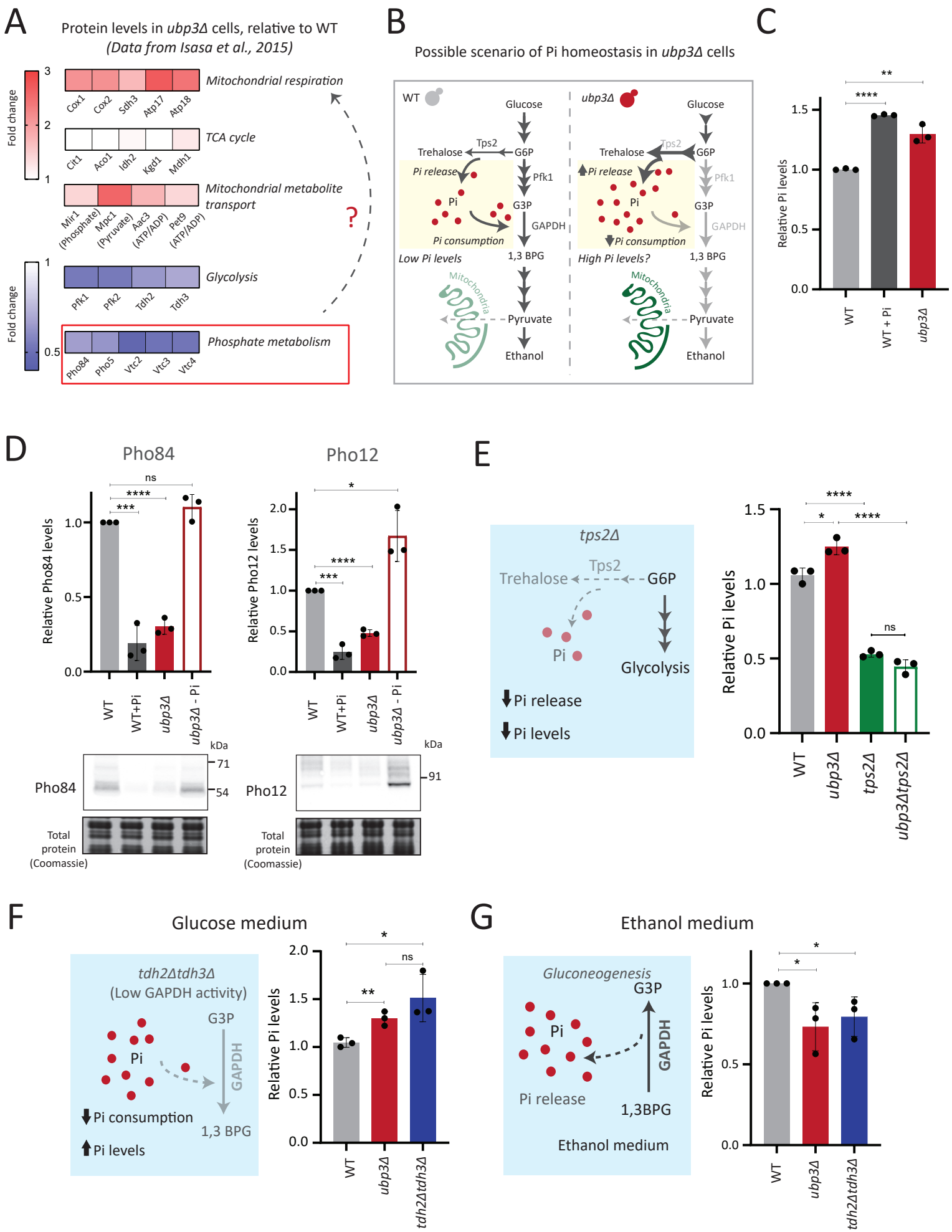

Figure 3: Rerouted glucose flux results in phosphate (Pi) accumulation

A) Changes in protein levels in *ubp3Δ* (dataset from Isasa et al., 2015). *ubp3Δ* cells have an increase in proteins involved in mitochondrial respiration and decrease in proteins involved in glucose and phosphate metabolism.

B) Schematic showing maintenance of Pi balance during glycolysis. Trehalose synthesis from G6P releases Pi, and the conversion of G3P to 1,3BPG by GAPDH consumes Pi. In *ubp3Δ*, trehalose biosynthesis (which releases Pi) increases. *ubp3Δ* have decreased GAPDH, which will decrease Pi consumption. This increase in Pi release along with decreased Pi consumption could increase cytosolic Pi.

C) Intracellular Pi levels in WT and *ubp3Δ*. WT and *ubp3Δ* were grown in high glucose and the total free phosphate (Pi) levels were estimated. WT in high Pi (2% glucose, 10mM Pi) was a positive control. Data represent mean ± SD from three biological replicates (n=3). Also see figure S3A.

D) Pho regulon responses in WT and *ubp3Δ*. Protein levels of Pho84-FLAG and Pho12-FLAG were compared between WT grown in high glucose and in high Pi, *ubp3Δ* in high glucose with or without a shift to a no-Pi medium for one hour, by western blot. A representative blot (out of three biological replicates, n=3) and their quantifications are shown. Data represent mean ± SD.

E) Contribution of trehalose synthesis as a Pi source. WT, *tps2Δ*, *ubp3Δ,* and *ubp3Δtps2Δ* were grown in high glucose and the total Pi levels were estimated. Data represent mean ± SD from three biological replicates (n=3). Also see figure S3B.

F) Loss of GAPDH isozymes Tdh2 and Tdh3 and effect on Pi. WT, *ubp3Δ,* and *tdh2Δtdh3Δ* were grown in high glucose and total Pi was estimated. Data represent mean ± SD from three biological replicates (n=3).

G) Pi levels in *ubp3Δ* and *tdh2Δtdh3Δ* cells in ethanol medium. WT, *ubp3Δ,* and *tdh2Δtdh3Δ* cells were grown in ethanol medium and the total Pi levels were estimated. Data represent mean ± SD from three biological replicates (n=3).

Data information: *p<0.05, **p<0.01, ***p<0.001, ****p<0.0001.

Figure 4: Mitochondrial Pi availability correlates with mitochondrial activity in *ubp3Δ*

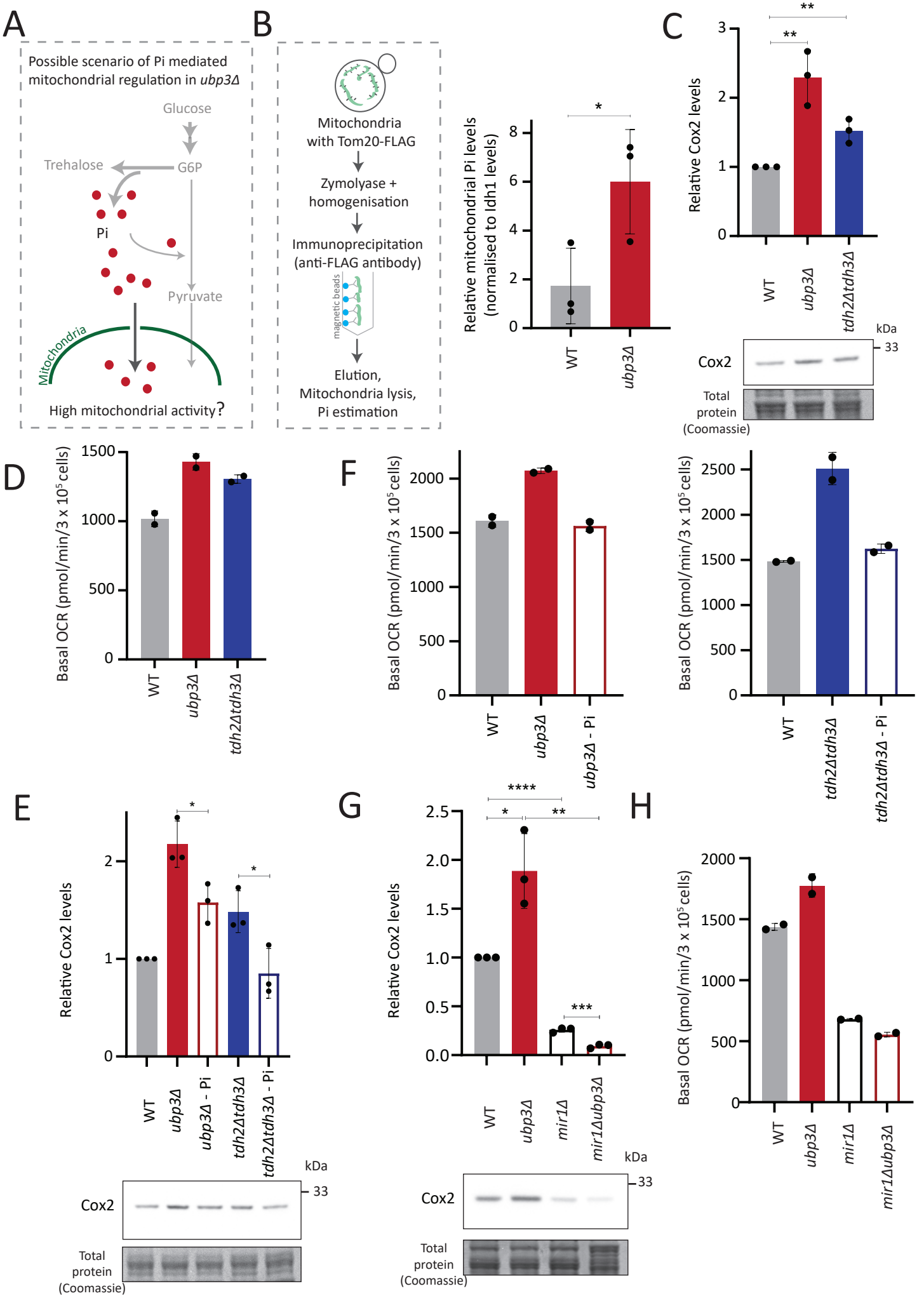

Figure 4: Mitochondrial Pi availability correlates with mitochondrial activity in *ubp3Δ*

A) A hypothetical mechanism of cytosolic free Pi controling mitochondrial activity by regulating mitochondrial Pi availability.

B) Mitochondrial Pi amounts in WT vs *ubp3Δ*. Mitochondria were isolated by immunoprecipitation from WT and *ubp3Δ* and mitochondrial Pi estimated. Mitochondrial Pi levels (normalised to Idh1) are shown. Data represent mean ± SD from three biological replicates (n=3). Also see figure S4A, B.

C) Cox2 protein in *tdh2Δtdh3Δ*. WT, *ubp3Δ,* and *tdh2Δtdh3Δ* were grown in high glucose and Cox2 protein was estimated. A representative blot (out of three biological replicates, n=3) and their quantifications are shown. Data represent mean ± SD.

D) Basal OCR levels in *tdh2Δtdh3Δ*. WT, *ubp3Δ,* and *tdh2Δtdh3Δ* were grown in high glucose and basal OCR was measured from two independent experiments (n=2). Data represent mean ± SD. Also see figure S4C.

E) Comparative Pi amounts and Cox2 levels in *ubp3Δ*, *tdh2Δtdh3Δ,* WT cells. WT cells were grown in high glucose, *ubp3Δ* and *tdh2Δtdh3Δ* were grown in high glucose and low Pi, and Cox2 protein was estimated. A representative blot (out of three biological replicates, n=3) and their quantifications are shown. Data represent mean ± SD. Also see figure S4D, S4F.

F) Pi amounts and basal OCR in *ubp3Δ* and *tdh2Δtdh3Δ* vs WT cells. WT cells were grown in high glucose, *ubp3Δ* and *tdh2Δtdh3Δ* were grown in high glucose and low Pi, and basal OCR was measured from two independent experiments (n=2). Data represent mean ± SD.

G) Effect of loss of mitochondrial Pi transporter Mir1 on Cox2protein. WT, *ubp3Δ*, *mir1Δ,* and *mir1Δubp3Δ* were grown in high glucose and Cox2 amounts compared. A representative blot (out of three biological replicates, n=3) and their quantifications are shown. Data represent mean ± SD.

H) Relationship of mitochondrial Pi transport and basal OCR in WT vs *ubp3Δ*. WT, *ubp3Δ*, *mir1Δ,* and *mir1Δubp3Δ* cells were grown in high glucose and basal OCR was measured from two independent experiments (n=2). Data represent mean ± SD.

Data information: *p<0.05, **p<0.01, ****p<0.0001.

Figure 5: Mitochondrial Pi availability constrains mitochondrial activity under high glucose

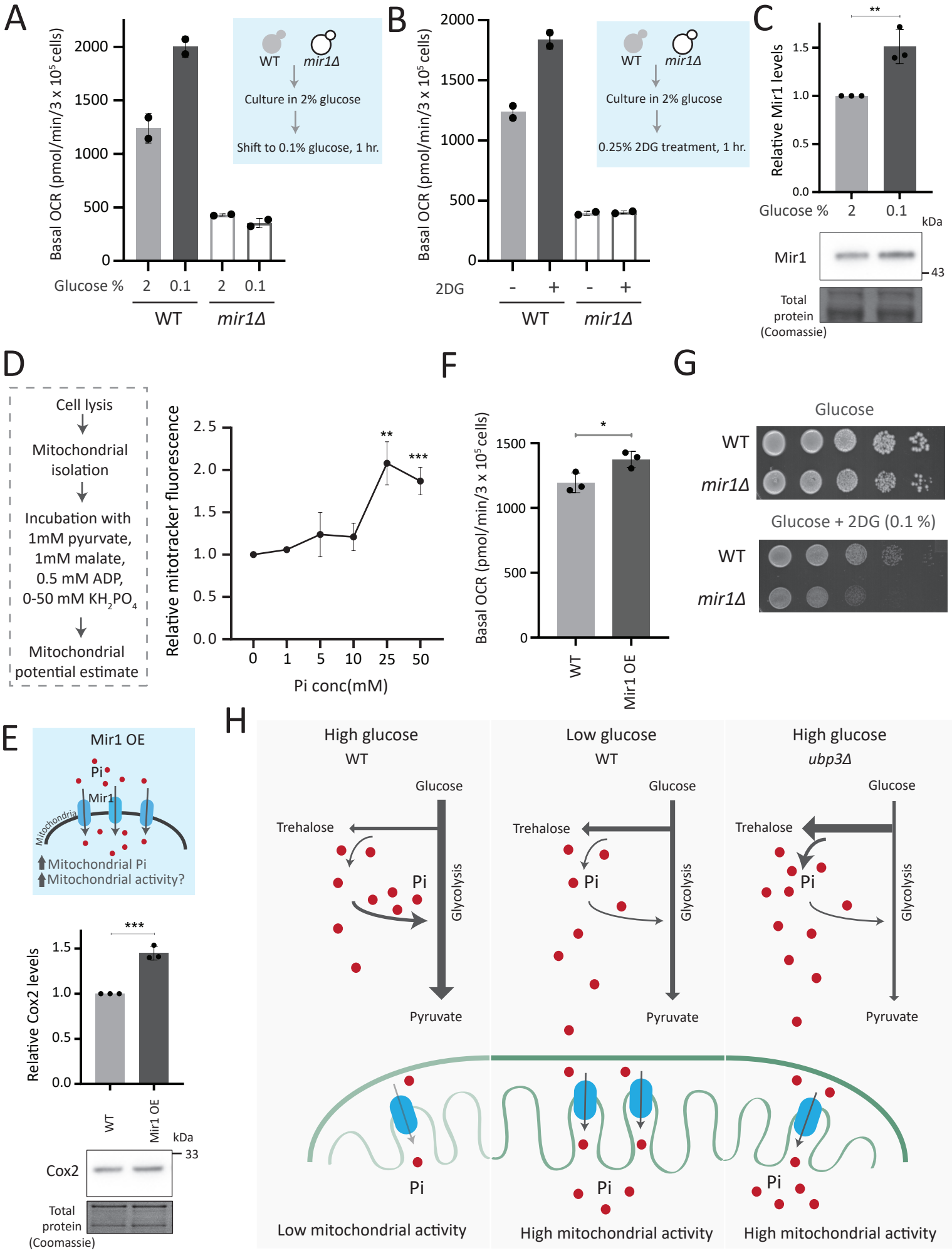

Figure 5: Mitochondrial Pi availability constrains mitochondrial activity under high glucose

A) Relationship of mitochondrial Pi transport and respiration after glucose removal. WT and *mir1Δ* cells were cultured in high (2%) glucose and shifted to low (0.1%) glucose for 1 hour. The normalized basal OCR, from two independent experiments (n=2) are shown. Data represent mean ± SD.

B) Requirement of mitochondrial Pi transport for switch to respiration upon glycolytic inhibition by 2DG. WT and *mir1Δ* cells were cultured in high glucose and treated with or without 0.25% 2DG for 1 hour. Basal OCR was measured from two independent experiments (n=2). Data represent mean ± SD. Also see figure S5A.

C) Glucose-dependent regulation of Mir1. Cells (with Mir1-HA) were grown in high glucose and shifted to low glucose (0.1% glucose) for 1 hour, and Mir1 levels compared. A representative blot (out of three biological replicates, n=3) and their quantifications are shown. Data represent mean ± SD. Also see figure S5B.

D) Increasing Pi concentrations and mitochondrial activity in isolated mitochondria. Mitochondria were isolated from WT cells grown in high glucose, incubated with 1 mM pyruvate, 1 mM malate, 0.5 mM ADP and 0-50 mM KH_2PO_4. The mitochondrial activity was estimated by mitotracker fluorescence intensity, and intensities relative to the sample with 0 mM KH_2PO_4 is shown. Data represent mean ± SD from three biological replicates (n=3).

E) Effect of overexpressing Mir1 on Cox2 protein. WT (containing empty vector) and Mir1 overexpressing (Mir1OE) cells were grown in high glucose and Cox2 levels were estimated. A representative blot (out of three biological replicates, n=3) and their quantifications are shown. Data represent mean ± SD. Also see figure S5F.

F) Effect of overexpressing Mir1 on basal OCR. The basal OCR in WT (containing empty vector) and Mir1OE in high glucose was measured from three independent experiments (n=3). Data represent mean ± SD.

G) Mitochondrial Pi transport requirement for growth after 2DG treatment. Shown are serial dilution growth assays in high glucose in the presence and absence of 0.1% 2DG, using WT and *mir1Δ* cells. The results after 40hrs incubation/30°C are shown.

H) A model illustrating how mitochondrial Pi availability controls mitochondrial activity. In high glucose, the decreased Pi due to high Pi consumption in glycolysis, along with the glucose-mediated repression of mitochondrial Pi transporters, decreases mitochondrial Pi availability. This reduces mitochondrial activity. In low glucose, increased mitochondrial Pi transporters and lower glycolytic flux increases mitochondrial Pi, leading to enhanced mitochondrial activity. In *ubp3Δ* cells in high glucose, high trehalose synthesis and lower glycolytic flux results in an increase in Pi. This increases mitochondrial Pi availability and thereby the mitochondrial activity.

Data information: *$p<0.05$, **$p<0.01$, ***$p<0.001$.